Integrated Attitude and Shape Control for OrigamiSats with Variable Surface Reflectivity

Bonar Robb[a,1,*], Aloisia Russo[c], Stefania Soldini[b], Paolo Paoletti[b], Juan Reveles[c], Gilles Bailet[a], Colin R. McInnes[a]

[a] *Space and Exploration Technology Group, James Watt School of Engineering, University of Glasgow, Glasgow, Scotland,*
[b] *University of Liverpool, Department of Mechanical, Materials and Aerospace Engineering, Liverpool, United Kingdom*
[c] *Oxford Space Systems, Oxford, United Kingdom*

Abstract

OrigamiSats, a new concept in solar sailing, are origami spacecraft with reflective panels that, when flat, operate as a conventional solar sail. Shape reconfiguration, i.e. "folding" of the origami design, allows the OrigamiSat to change operational modes, performing different functions as per mission requirements. For example, a flat OrigamiSat could be reconfigured into the shape of a parabolic reflector, before returning to the flat configuration when required to operate again as a solar sail, providing propellant-free propulsion. The attitude dynamics and shape reconfiguration of OrigamiSats are known to be highly coupled, thus presenting a challenge from a control perspective. This paper investigates the problem of integrating attitude and shape control of a Miura-fold pattern OrigamiSat through the use of variable reflectivity, allowing differences in solar radiation pressure to be used to enact shape reconfiguration and attitude manoeuvres. A closed-loop feedback controller is presented which combines and balances the attitude and shape control requirements, and gain-scheduling is implemented to address some specific features of the system dynamics. Numerical simulations of the multibody dynamics of the system are used to test the proposed controller and simulations of some example manoeuvres are performed which demonstrate the system's performance.

1. Introduction

The OrigamiSat concept is a new design paradigm in solar sailing, in which origami based designs are used to create reconfigurable and multifunctional membrane spacecraft. Russo et al. investigated the concept in Ref. [1], which described a potential swarm mission concept, investigated the multibody dynamics of OrigamiSats, and presented an investigation into the manufacturing of a prototype system. Reference [1] introduced the concept of Solar Radiation Pressure (SRP) induced folding of OrigamiSats, through the use of reflectivity control devices (RCDs) embedded in the OrigamiSat panels which allow the local reflectivity of each panel to be controlled, varying the acceleration due to SRP and folding the OrigamiSat in a controlled fashion. RCDs are a proven form of attitude control for solar sails, being used on the IKAROS solar sail demonstration mission [2]. Such devices offer fuel free attitude control, and additionally have very low power requirements, on the order of mW/cm^2 of RCD surface [3], and are being actively studied as attitude control systems for future solar sail mission proposals. Some recent examples include the work of Basseto et al. [4] and Boni et al. [5], who studied the use of RCDs for the attitude control of the Helianthus mission proposal, demonstrated a sliding mode control strategy [4] and investigated the structural response of a square solar sail during attitude manoeuvres [5]. Though some preliminary work attempting to implement closed loop control of OrigamiSat shape reconfiguration with RCDs was presented in Ref. [1], it was identified that shape

*Corresponding author
[1] Currently at London South Bank University
[2] An earlier version of this paper was presented at the 73rd IAC, Paris, France in September 2022. Paper number: IAC-22/C2/9.2x69275

reconfiguration through the use of SRP alone (i.e. without further actuation of some form in the panel hinges) would be challenging from a control perspective, due to the complex multibody dynamics, underactuated nature of the problem, and coupling between shape reconfiguration and the spacecraft attitude. Similar to the OrigimaSat concept, though at a smaller length-scale, is the recent work of Xie et al. [6] and Ren et al. [7], who proposed and prototyped a reconfigurable "ChipSail" solar sail system for sub-gram spacecraft. The proposed ChipSail achieves reconfiguration through the electrothermal actuation of bilayer metallic beams embedded in in the sail material as opposed to the SRP-induced reconfiguration strategy that is considered here for OrigamiSats.

The attitude control and shape reconfiguration of multibody spacecraft has been well studied in the literature for a variety of scenarios/spacecraft architectures, and using a range of modelling approaches. Trovarelli et al. demonstrated the attitude control of planar [8] and 3D [9] multibody systems using momentum preserving internal torques, demonstrating reorientation manoeuvres of linked bars/panels using hinge torques, finding optimal control solutions for these manoevures, and investigating the effect of collision or impingement constraints on the optimal control solutions. Similar work includes that of Gong et al., who also demonstrated attitude control through the use of shape reconfiguration for microsatellites [10] and femtosatellites [11], with the latter work including the design and testing of a foldable PCBsat. Ashrafiuon and Erwin [12] presented an approach for the design of sliding mode control for underactuated, nonlinear multibody systems, proving the stability of the closed-loop control system through Lyapunov stability analysis for certain conditions, and demonstrating simulation results for the control of an inverted pendulum and a multibody communication satellite. Though the method proposed here by Ashrafiuon and Erwin is clearly extendable to many different multibody spacecraft architectures, the same approach cannot be adopted for OrigamiSats because the system is non-conservative, as the force due to SRP introduces momentum to the system. While the OrigamiSat concept is quite new, there are some examples of similar multi-body membrane spacecraft to be found. Gong et al. [13] proposed the relatively similar concept of a multibody solar sail, comprised of four pivoting triangular sail "wings" mounted on a central bus, and demonstrated attitude manoeuvres through controlled pitching of each wing. Sinn and Vasile [14] investigated the multibody dynamics of a membrane structure consisting of inflatable cells, which is capable of shape reconfiguration. While similar in purpose to an OrigamiSat, the method of actuation and modelling is quite different to the approach taken in this paper.

A key difference between these previously studied systems and the control strategy proposed in [1] and studied further in this paper is that the RCD-controlled OrigamiSat system is underactuated and non-conservative, as SRP introduces angular momentum to the system. Therefore, some previously proposed strategies for multibody spacecraft control are not suitable for this problem. Due to the complexity of the system dynamics and underactuation, it is unlikely that a straightforward solution for the general OrigamiSat SRP control problem (i.e., a strategy that may be applied to any Origami folding pattern) is achievable, though it is possible that some general results and guidance for controller design can be gained by studying specific scenarios. Therefore, the aim of this paper is to present an investigation into OrigamiSat SRP controllability through the use of numerical simulations of a Miura-fold OrigamiSat. The Miura-fold represents a relatively simple Origami structure, in that there is only one degree of freedom in folding.

The paper is organised as follows. In Sec. 2 the approach to mathematically modelling OrigamiSats, first put forward in Ref. [1], is summarised (with some further details of the software implementation), and the OrigamiSat folding patterns which are used in later simulations are described. Then, Section 3 discusses the proposed control strategy and design of a closed-loop feedback controller that combines shape and attitude control. Results of simulation for some example manoeuvres are presented and discussed in Sec. 4, while the significance of the results and possibility of extending the strategy to other OrigamiSat designs are discussed in Sec. 5, along with the paper conclusions.

2. OrigamiSat Modelling

The OrigamiSats are modelled as a multibody system of rigid, flat panels (facets), linked by spherical joints placed at the vertices of the origami pattern's fold lines. The mathematical model is given in Ref. [1],

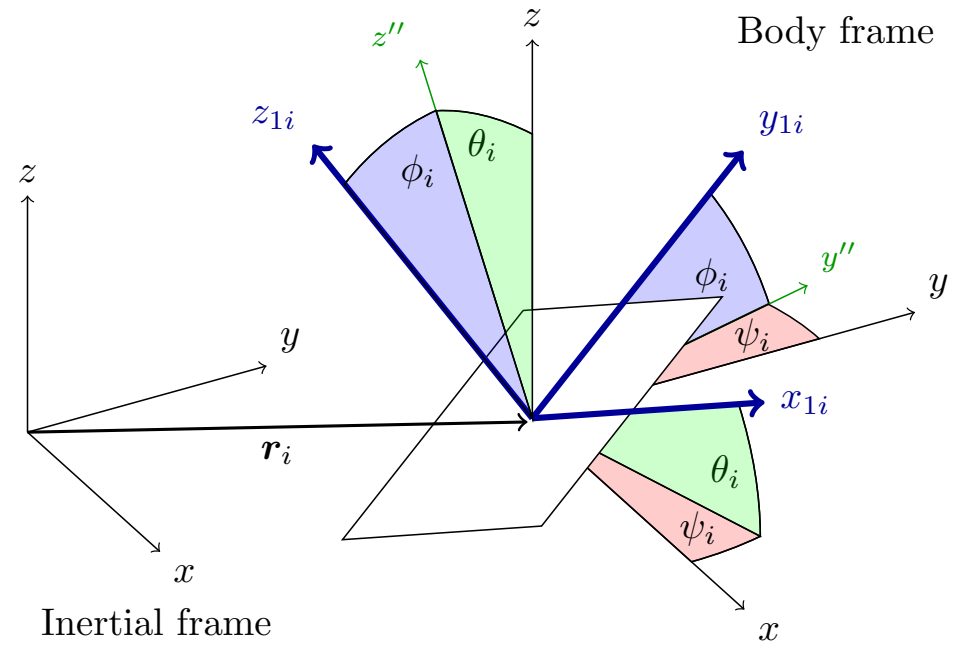

Figure 1: Sequence of rotations between the inertial frame xyz and the ith facet body frame $x_{1i}y_{1i}z_{1i}$

with the main equations repeated here for clarity of discussion. The dynamics of the multibody system are described using the well-known "augmented formulation" described by [15]:

$$\begin{bmatrix} \mathbf{M} & \mathbf{J}^T \\ \mathbf{J} & 0 \end{bmatrix} \begin{bmatrix} \ddot{\boldsymbol{q}} \\ \boldsymbol{\lambda} \end{bmatrix} = \begin{bmatrix} \boldsymbol{Q}_a + \boldsymbol{Q}_v \\ \boldsymbol{Q}_c \end{bmatrix} \tag{1}$$

where $\mathbf{M}$ is the system mass matrix, $\boldsymbol{q}$ the state vector of body coordinates and $\mathbf{J} = \partial \boldsymbol{C}/\partial \boldsymbol{q}$ is the constraint Jacobian, for the vector of system constraint equations $\boldsymbol{C}$. $\boldsymbol{\lambda}$ is a vector of Lagrange multipliers, used to solve for the constraint forces $\boldsymbol{Q}_c$, while $\boldsymbol{Q}_a$ and $\boldsymbol{Q}_v$ are the applied and inertial force vectors, respectively.

The state vector $\boldsymbol{q}$ contains the Cartesian coordinates of each facet's centre-of-mass, $\boldsymbol{r}_i$, and the three $ZY'X''$ Euler angles, ψ, θ, ϕ, describing its orientation relative to the inertial xyz frame. Figure 1 shows the reference frames, Euler angles and sequence of rotations for the ith facet. The state vector $\boldsymbol{q}$ is then ordered such that $\boldsymbol{q} = [x_1, y_1, z_1, \psi_1, \theta_1, \phi_1, ..., x_N, y_N, z_N, \psi_N, \theta_N, \phi_N]^T$, where N is the total number of facets. The mass matrix $\mathbf{M}$ is composed diagonally by $[m_1\mathbf{I}_{3\times3}, \mathcal{I}_1, ..., m_N\mathbf{I}_{3\times3}, \mathcal{I}_N]$, where $\mathbf{I}_{3\times3}$ is the three by three identity matrix, while m_i and $\mathcal{I}_i$ are the mass and inertia tensor (in the body frame) of the ith facet, respectively.

The constraint equations vector $\boldsymbol{C}$ are generated through symbolic computation in a Mathematica program, which takes as its input a nested list of the panel vertex coordinates (which defines the Origami fold pattern) and generates the constraints following the equations given in Ref. [1] (Eq. 16-17 and the surrounding discussion). For an initial state vector $\boldsymbol{q}$ and applied force vector $\boldsymbol{Q}_a$, the differential algebraic system of equations in Eq. 1 is solved for the Lagrange multipliers $\boldsymbol{\lambda}$, and the accelerations $\ddot{\boldsymbol{q}}$, which are then numerically integrated in MATLAB to simulate the system dynamics. The applied forces due to SRP are determined using the ray-tracing method developed in Ref. [1], which allows any shadowing or inter-panel reflections to be taken into account when determining the force on each panel. Panel forces are determined from the ray-tracer output of ray interception/reflection points, and are given by:

$$\boldsymbol{F}_i^{SRP} = P \sum_j \text{sign}(\boldsymbol{u}_j \cdot \boldsymbol{n}) \left(\frac{D_R}{N_R}\right)^2 \left[\prod_c \rho_c^j\right] \times ((1+\rho_i)\cos\alpha \boldsymbol{n} + (1-\rho_i)\sin\alpha \boldsymbol{t}) \tag{2}$$

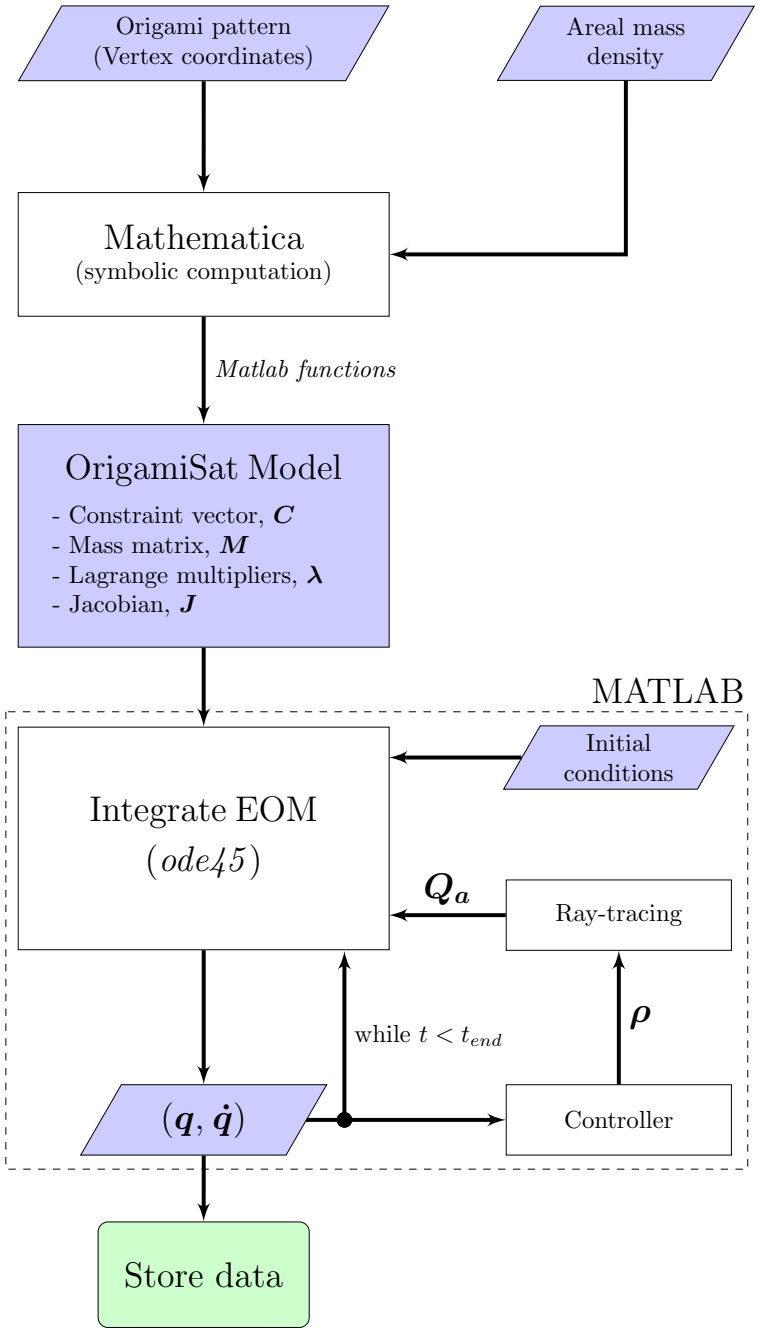

Figure 2: Flow chart of the software implementation of the OrigamiSat multibody dynamics equation generation and numerical simulation

which calculates the force due to SRP from each intercepted ray, assuming the panel is a Lambertian surface and the incoming radiation is specularly reflected/absorbed (according to the panel reflectivity ρ_i). $P = 4.563 \times 10^{-6}$ N m^{-2} is the SRP constant at 1 AU from the Sun, $\boldsymbol{u}_j$ is the vector in the direction of ray j, $\boldsymbol{n}$ and $\boldsymbol{t}$ are the facet normal and transverse directions, respectively. Equation 2 is found by replacing the total facet area with $D_R^2/N_R^2 \prod_c \rho_c^p / \cos\alpha$, which represents the area illuminated by ray j (where α is the angle between the incident ray and the facet normal) and thus ensures that the total intensity of light from

all rays sums to the total flux through a $D_R \times D_R$ square. The term $\prod_c \rho_c^j$ is the product of the reflectivity of all facets previously intercepted by ray j, which takes into account the reduced intensity of a reflected ray due to imperfect surface reflectivity. Further details of the ray-tracing method and derivation of Eq. 2 are provided in Ref. [1]. A flow chart of the software implementation of the model is given in Fig. 2, showing the separation between model generation (Mathematica) and the numerical integration and force calculations (MATLAB).

3. Integrated Shape and Attitude Control for OrigamiSats

In this section a control logic is proposed for integrating the attitude and shape control of an OrigamiSat through the use of variable reflectivity facets. In principle, the reflectivity of the OrigamiSat facets could be controlled through the use of RCDs, a proven technology for solar sails with their use for attitude control demonstrated on the IKAROS mission [2]. In Ref. [1], shape control through variable reflectivity was demonstrated for a pyramidal OrigamiSat, with a PD control law implemented. In this case, however, the attitude dynamics were decoupled from the shape control strategy by constraining the central panel of the sail to always remain sun-pointing. Now, a control law is sought that integrates attitude control with shape reconfiguration for an unconstrained OrigamiSat in free space. A Miura-fold pattern is selected as a test case for the control design. This origami pattern represents a simplified case (in terms of the Origami kinematics), as the system has only one degree of freedom in folding (in addition to the three degrees of freedom in rotation). The Miura-fold is also a well known design, and has tesselation properties, so the system could potentially be scaled to a greater number of panels. The shape and attitude of the Miura-fold OrigamiSat are still coupled however, and so even as a simplified case the system remains challenging from a control perspective. Furthermore, since there is only one folding degree-of-freedom, study of this design is hoped to provide a greater qualitative understanding of the nature of the attitude/shape coupling of the system, and thus provide some deeper insight into the controller performance which could in the future be applied to more complex OrigamiSat designs.

3.1. Control challenges

As noted in the introduction, the system dynamics are coupled and the system is underactuated, as changing the panel reflectivity has a limited effect on the change in direction or magnitude of the force due to SRP. Nevertheless, it was found in Ref. [1] that the multibody dynamics of the system can be exploited to enact folding of the OrigamiSat, and that often the reflectivity pattern required to perform the desired "folds" could be intuited by considering opposing reflectivities for panels on either side of the required fold line. In the case of the Miura fold pattern, it was found that folding/unfolding of the pattern could be enacted by two opposite reflectivity patterns. While it is likely not always possible to simply guess the required reflectivity patterns, or even likely that there always exists a reflectivity pattern to perform the desired fold, for the relatively simple Miura pattern this approach is again adopted to simplify the integration of shape and attitude control. A further complication and added nonlinearity to the dynamics is the effect of interpanel shadowing or reflection, where the panel forces can change discontinuously as the OrigamiSat changes shape and different panels become illuminated. As this effect depends on both the (time-varying) OrigamiSat geometry and attitude, it is non-trivial to determine when or if interpanel reflections become a dominant contribution to the panel forces, and indeed these effects require the use of ray-tracing to accurately calculate the force due to SRP on the spacecraft. Again, however, for simple fold patterns it is possible to intuitively deduce or predetermine which configurations result in interpanel reflections and build this knowledge into the control design on a case-by-case basis. For the Miura fold, it was found that the configuration shown in Fig. 3 resulted in interpanel reflections that reversed the folding effect of the shown reflectivity pattern (light blue implies $\rho = 1$, dark blue $\rho = 0$), causing the sail to reopen due to the increase force on the outer panels. As noted earlier, RCDs are a proven technology for attitude control of solar sails. By varying the reflectivity of these devices mounted on a sailcraft, the force due to SRP is modified on the device and thus useful torques can be produced for attitude control purposes. In the case of OrigamiSats, it is assumed that the reflectivity of each panel can be controlled individually, and varied

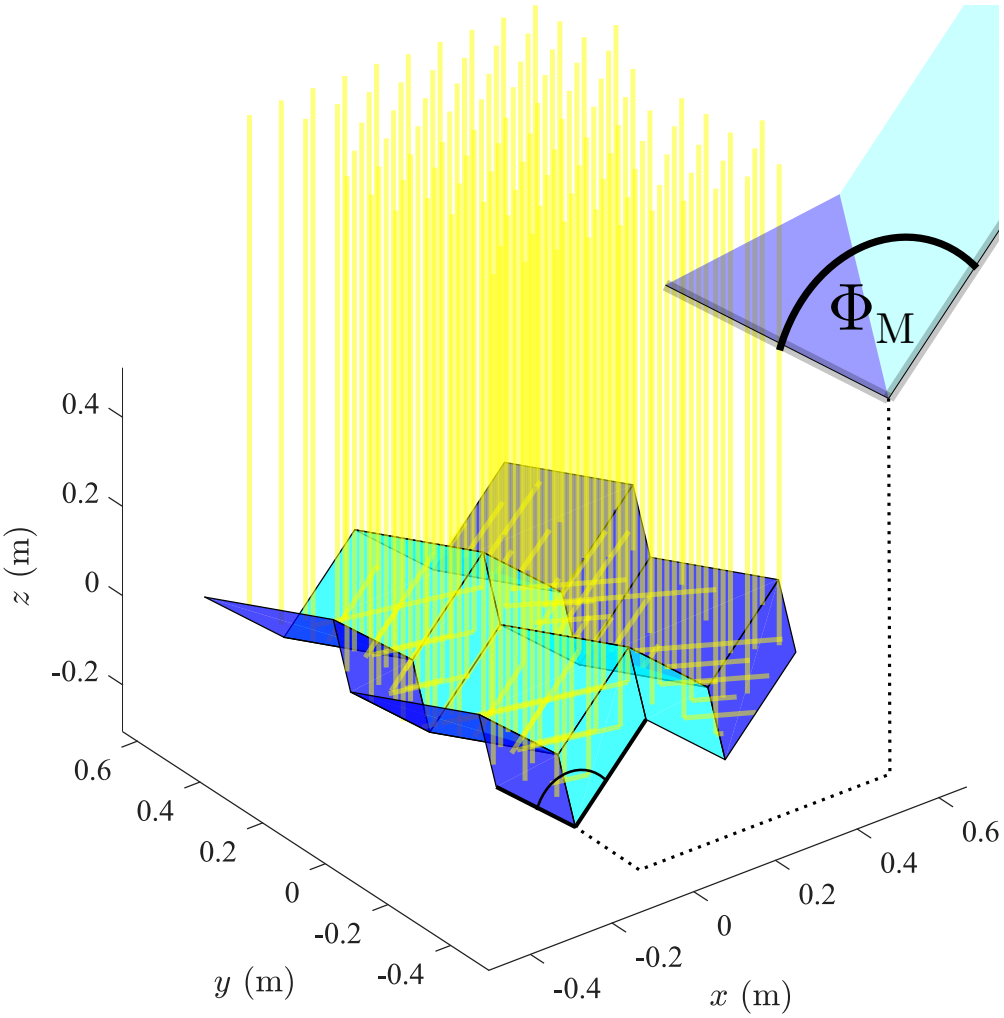

Figure 3: Interpanel reflections reverse the folding effect of some reflectivity patterns for a Miura OrigamiSat. Reference "Fold angle", Φ_M, highlighted.

between $\rho = 0$ (perfectly absorbing) and $\rho = 1$ (perfectly reflecting), which represents an ideal scenario. In practice, many RCDs have two discrete states, which are switched when a voltage is applied to the material. However, it would be possible to achieve intermediate values between 0 and 1 by having a large number of (discrete) RCDs on each panel, and switching a specified portion of them at a time. It was noted in the introduction that an advantage of the use of RCDs is their low power requirements, on the order of $\mathrm{mW/cm^2}$ [3]. Therefore even for the ideal OrigamiSat modelled here, in which the entire sail surface is assumed to have variable reflectivity, the power requirements of the system could be expected to be on the order of a few Watts and would thus not represent a signifiant contribution to a typical spacecraft's power requirements. Previously, attitude control through the use of an array of variable reflectivity panels was demonstrated by Borggräfe et al. [16] through simulations, though in this case the authors assumed discrete reflectivity states (0 or 1 for each cell), and determined the required reflectivity pattern by considering all possible reflectivity patterns. A lookup table was then created of all possible the generated torques, and compared with the desired reference torque output by the controller to find the necessary reflectivity pattern. While this strategy could also be employed for OrigamiSats, a limitation is that the number of possible patterns increases exponentially with the number of panels. Furthermore, imposing discrete states on the panels would complicate the shape/attitude control integration by not allowing the separate control signals to be

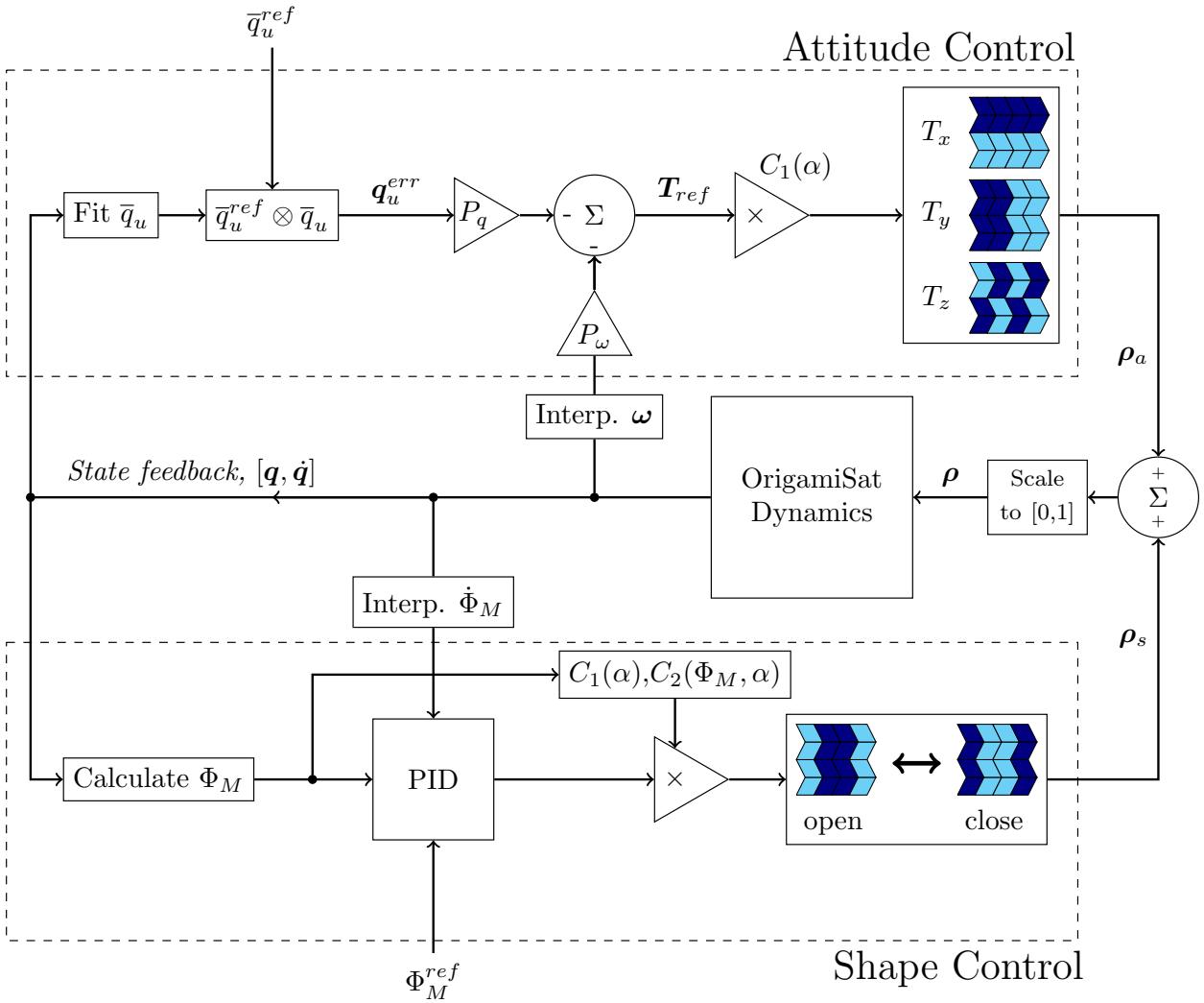

Figure 4: Block diagram of the closed-loop feedback controller

superimposed, as described in the following section.

3.2. Controller design

In this section, a closed-loop feedback controller for the shape and attitude of a Miura type solar sail is presented and analysed through numerical simulations. Shape reconfiguration is controlled through a classical PID control law, with the output signal used to produce a reflectivity pattern of panel reflectivity values for the sail. Simultaneously, a quaternion error feedback controller is used to generate a reference desired torque for attitude control, and a further reflectivity pattern is generated that is calculated to produce a torque as near to the reference as possible with the RCD panels. These two (shape and attitude) reflectivity patterns are then superimposed and applied to the OrigamiSat. While the control scheme is relatively straightforward (in terms of the individual control laws used), some further modifications are made to improve control performance and build in some knowledge of the system dynamics and nonlinearities which arise due to the multibody dynamics and interpanel reflections.

A block diagram of the controller is shown in Fig. 4, showing the separate attitude/shape control loops and their integration. For attitude control, first a quaternion representation is found from the OrigamiSat

panel coordinates by fitting a rotation between the initial panel centre of masses and the current positions (using singular value decomposition, following Ref. [17]). This quaternion is then input to the quaternion error feedback controller, along with the desired reference orientation and current body rates, found through backwards difference interpolation of the current rotation and that of the previous timestep. This produces a reference torque given by:

$$\boldsymbol{T}_{ref} = -P_q \boldsymbol{q}_u^{err} - P_\omega \boldsymbol{\omega} = \begin{pmatrix} T_x \\ T_y \\ T_z \end{pmatrix} \tag{3}$$

This is then used to produce a reflectivity pattern by superimposing three reflectivity patterns that are known to produce a torque in each of the body frame axes. The method here is similar to that proposed by Borgräffe et al. [16] for an RCD array, though here we consider the panel reflectivities to be continuously variable between 0 and 1, and thus the desired torque can be composed of a combination of the three basis patterns shown in Fig. 4. A further key difference is that the planar spacecraft considered by Borgräffe et al. was only capable of producing torques around the body x and y axes, but the Miura pattern OrigamiSat is capable of producing a torque in the z direction, as long as the sail is not perfectly flat. The "attitude reflectivity vector", where each element gives the desired reflectivity of the corresponding OrigamiSat panel, is given by:

$$\boldsymbol{\rho}_a = T_x \boldsymbol{\rho}_x + T_y \boldsymbol{\rho}_y + T_z \boldsymbol{\rho}_z \tag{4}$$

where $\boldsymbol{\rho}_{xyz}$ are the vectors corresponding to the patterns illustrated in Fig. 4 for the three torque axes if the corresponding torque component is positive, and the opposite patterns if it is negative.

Shape control is provided by a PID controller. First, the fold angle Φ_M is calculated from the OrigamiSat panel coordinates (the fold angle is highlighted in Fig. 3) and then fed into the PID controller, along with the desired fold angle, interpolated fold angle rate (again estimated with a backwards difference formula), and previous measurements to calculate the error integral. The controller output u_S, which physically represents the desired generalised foling force associated with the folding angle Φ_m, is given by:

$$u_S = k_p \Phi_E + k_i \int_0^\tau \Phi_E(\tau) d\tau + k_d \dot{\Phi}_E \tag{5}$$

where Φ_E is the error between Φ_M and the desired fold angle, while $k_{p,i,d}$ are the PID control gains. This is then converted to a reflectivity pattern, where again known patterns are used that correspond to folding and unfolding of the OrigamiSat (as demonstrated for the Miura sail in Ref. [1]). The shape control pattern is thus:

$$\boldsymbol{\rho}_s = u_S \boldsymbol{\rho}_f \tag{6}$$

where ρ_f is the "open" pattern depicted in Fig. 4 for u_S positive and "closed" for negative.

This results in two separate control outputs, $\boldsymbol{\rho}_a$ and $\boldsymbol{\rho}_s$, which are vectors of positive values corresponding to the panel reflectivities (though at this point the raw values may exceed 1).

3.3. Gain-Scheduling

The control outputs u_s and $\boldsymbol{T}^{ref}$, from Eqs. 3 and 5, respectively, are further modified by some gain scheduling functions. Gain scheduling modifies the control gains in different operation regions, as determined by some preset values based on measured scheduling parameters, and is therefore a simple method of dealing with the nonlinear dynamics of the system if there are certain known or determined features. The required scheduling functions were deduced by performing simulations of different manoeuvres and addressing obvious points of failure for the controller. Two scheduling parameters are used, the first being Φ_M, the fold angle, and the second being the sail pitch angle, α, which is the angle between the incident radiation, and the sail normal (body z-axis). Two scheduling functions, C_1 and C_2, are implemented, such that the overall panel reflectivity vector is given by:

$$\boldsymbol{\rho} = C_1(\alpha) \left[C_2(\Phi_M, \alpha) u_s \boldsymbol{\rho_f} + T_x \boldsymbol{\rho_x} + T_y \boldsymbol{\rho_y} + T_z \boldsymbol{\rho_z} \right] \tag{7}$$

The first of the gain-scheduling functions is given by:

$$C_1 = \begin{cases} 1 & \text{if } \alpha < 90^\circ \\ -1 & \text{otherwise} \end{cases}$$

which ensures that the reflectivity pattern is reversed for angles of incidence greater than 90°. This is required as the effect of the reflectivity patterns is reversed depending on which side of the sail is illuminated (where it is assumed that both sides of the panels are fitted with RCD devices). The second scheduling function modifies the shape/folding output only, and is given by:

$$C_2 = \begin{cases} (\Phi_M - 170)^2 + 1 & \text{if } \Phi_M > 170^\circ \\ 1 & \text{if } 170^\circ > \Phi_M > 114^\circ \\ 0 & \text{if } \Phi_M < 114^\circ \text{ and } \alpha > 90^\circ \end{cases}$$

Due to the interpanel reflections depicted in Fig. 3, the reflectivity pattern used to close the sail loses effectiveness when the fold angle is below 114° (determined through simulation). Therefore, further attempts to close the sail beyond this angle are counterproductive, and it is better to rely on any remaining folding momentum to achieve smaller fold angles. This is only required for $\alpha < 90^\circ$, where folding is achieved by setting the inner panels to $\rho = 1$ (and so the Miura pattern is folding towards the incident radiation). For folding in the opposite direction, i.e., where the outer panels have $\rho = 1$, interpanel reflections are not a concern and folding can be enacted in the full range of Φ_M. Above $\Phi_M = 170^\circ$, C_2 is set to the given quadratic, to rapidly increase the shape-control gain when the sail approaches the perfectly flat condition. This factor was included as the sail is restricted to not exceed a fold angle of 180°, where the Miura pattern becomes perfectly flat and folds can be induced around incorrect fold lines. In practice, it would be possible to design a Miura fold pattern that could reverse folding directions around 180°, using mechanical hinges or creased folding lines that would ensure the correct folds are maintained at this point of reversal. In the simulation however it was found that the perfectly flat condition often led to computational instability, and therefore incorporating reversible folding would require some modification to the constraint equations. C_2 instead ensures that, for angles above 170°, the shape control gain is increased significantly and the controller favours shape control over attitude in this region - since the desired attitude control pattern may act to further unfold the OrigamiSat in this configuration. As noted, the predefined reflectivity patterns $\boldsymbol{\rho}_{f,x,y,z}$ which appear in Eq. 7 are one of two vectors/patterns depending on the sign of the control signal with which they are multiplied. For positive values of C_1, C_2 and u_s, $\boldsymbol{\rho}_f$ is the "open" pattern shown in Fig. 4, and for negative values the opposite, and equivalent for the components of $\boldsymbol{T}^{ref}$ and corresponding patterns. Equation 7 then gives a vector of positive values corresponding to the desired reflectivity of each

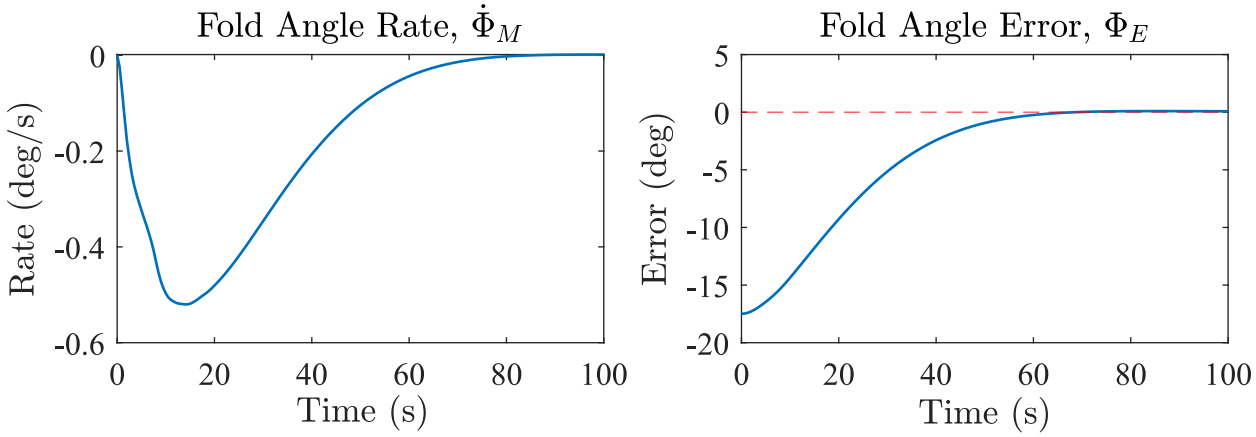

Figure 5: PID tuning of shape control law for Miura fold OrigamiSat.

panel, and as a final step the values are scaled to lie between $[0, 1]$, by dividing all values by the value of the largest element (if the maximum is greater than 1). This scaling then automatically balances the attitude/shape control requirements at a given moment, where the weighting for each is determined by the magnitude of the control signals output by each block of the controller.

Table 1: Simulation data.

Side length		1 m
Areal Mass Density		10 g/m^2
Simulation timestep	dt	0.1 s
Simulation time		1000 s
Number of rays	N_R	500^2
Control gains	P_q	15
	P_ω	1000
	k_p	0.48
	k_i	0.0069
	k_d	8.4

3.4. Controller Tuning

The shape PID-control gains are tuned following the well-known Zeigler-Nichols method (e.g. [18]), where first the integral and derivative gains are set to zero, and the proportional gain is increased until

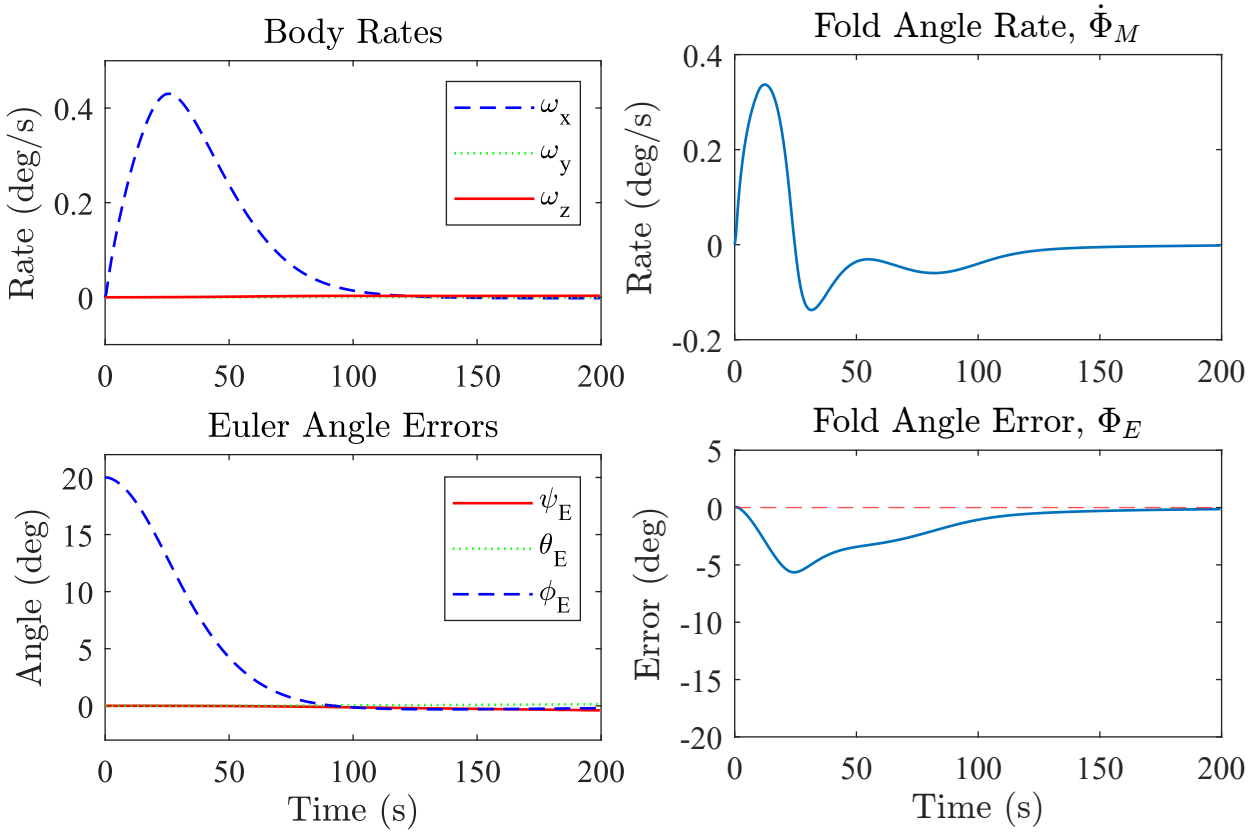

Figure 6: Attitude and shape response during 20° slew manoeuvre.

steady oscillations are seen in the response. The gains are then set in relation to this following the standard equations. The control response for a desired fold of 20° is shown in Fig. 5. The fold angle is seen to smoothly fall to the set point, though there is not the expected overshoot and settling that would be expected following Zeigler-Nichols tuning. This is likely due to the nonlinearity of the folding process, in that the "unfolding" reflectivity pattern results in a greater acceleration of the folding angle than the "folding" pattern. Despite this, the selected gains were found to perform well enough, and in fact it may be desirable to have no overshoot in the response as it is known that beyond some fold angles the controller loses effectiveness due to the interpanel reflections illustrated in Fig.3. The attitude control gains are selected by adjusting P_q and P_w to produce an output that is comparable to the shape control output for similar error values, so that there is nominally an equal weighting given to the two control signals, and the available reflectivity control is evenly split between both requirements. The system response for a 20° slew manoeuvre around the body x-axis is shown in Fig. 6, again showing that the response is smooth and with no overshoot. While performing the manoeuvre, the shape becomes disturbed due to the coupling of the multibody system. The fold angle disturbance and recovery is shown in Fig. 6, showing that there is a relatively large disturbance of approximately 5° in the fold angle, but this is then corrected by the shape-controller over the remainder of the simulation. The control gains, spacecraft data, and simulation parameters are summarised in Table. 1.

4. Demonstration of Integrated Shape and Attitude Control

The control law is now demonstrated through simulations of two example manoeuvres. The two manoeuvres are illustrated in Fig. 7. The first is comprised of a rotation of 180° around the body x-axis, while simultaneously folding the sail to a fold angle of 140°. The second manoeuvre is a 90° rotation around the z-axis, again while folding to an angle of 140°. This manoeuvre demonstrates how the sail can generate a torque in the z-direction with the given pattern, but only when the sail is not perfectly flat so that some panel surfaces are at an angle to the xy frame. Figure 7 shows the sail plotted at 200 s intervals during the simulation. The panel reflectivities are also shown, ranging from light to dark blue, corresponding to perfectly reflective and absorbing respectively. Plots of the sail angles, rates and control signals are shown in Figs 8 and 9. In both cases the desired attitude is approached smoothly, while the shape configuration is less smooth with larger disturbances during the manoeuvre. Plots of the control signals are given for both before and after the scaling process, demonstrating the relative values of the shape and attitude control outputs and how these are balanced at different points of the simulation. Initially, the fold angle is greater than 170°, and so shape-control is favoured (due to the quadratic C_2 function described previously). Once the angle falls below 170°, both the shape and attitude signal are roughly equal in magnitude, and so the two objectives share the scaled control values evenly. For the first manoeuvre, as shown in Fig. 8, there is a period after 200 s where the shape control signal dominates the scaled values. This is the point where the sail approaches a rotation of 90°, and so is nearly side-on to the incident radiation. The force due to SRP is therefore much lower in this configuration, and the system loses control effectiveness, hence the large errors in fold angle. Once reaching the desired attitude and shape, the fold angle error is approximately 0.02 degrees for both manoeuvres.

In practice, the direction of the thrust produced by each facet will be affected by a number of factors not taken into consideration by the model used here, such as curvature of the facet surfaces, vibration modes, and wrinkling of the sail material. For the rigid facets being considered here it is expected that wrinkling and membrane curvature will be less of a concern than for traditional solar sail designs (as suggested by the physical prototyping presented in Ref. [1]), though it is still likely that deviations from the ideal model will occur. Further considerations could be sensor noise, and the challenge of accurately measuring the orientations of the facets during operation. To test the controller in the presence of such perturbations and noise, the second manoeuvre was repeated with the inclusion of an unknown perturbation to the panel forces added at each timestep. The perturbation is calculated by adding a random noise vector, $\boldsymbol{r}_N = [x_N, y_N, z_N]$ to the panel body forces, $\boldsymbol{F}_i^{SRP}$ which are calculated from the ray-tracer output and Eq. 2. Then, x_N, y_N, and z_N are taken from a normal distribution with standard deviation equal to 10% of $|\boldsymbol{F}_i^{SRP}|$, such that $\boldsymbol{r}_N$ is likely to have a magnitude less than 10% of the originally calculated force vector, and perturb the

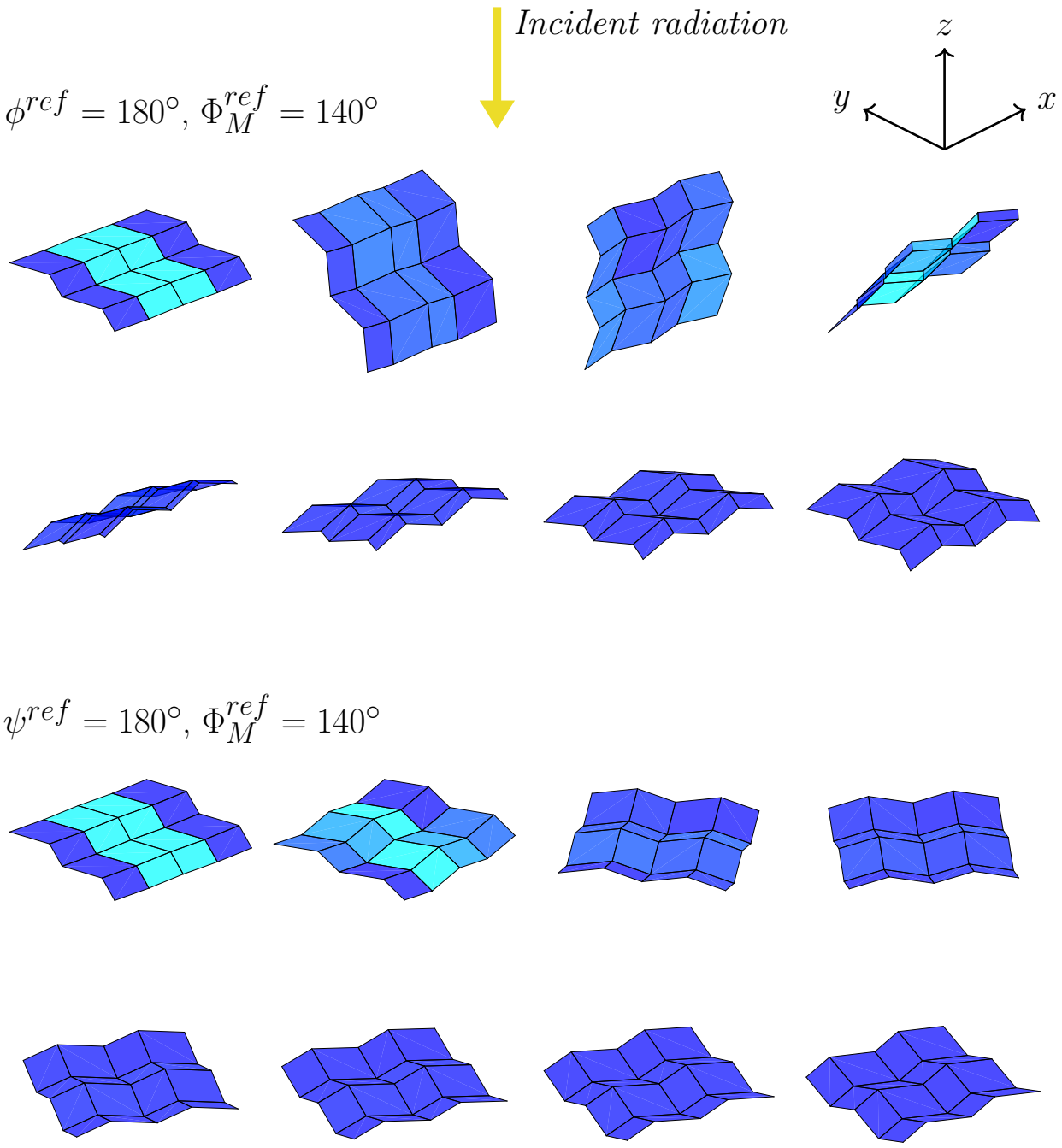

Figure 7: Miura OrigamiSat plotted at 200 s intervals for the two example manoeuvres. Light and dark blue represent perfectly reflecting/absorbing panels respectively.

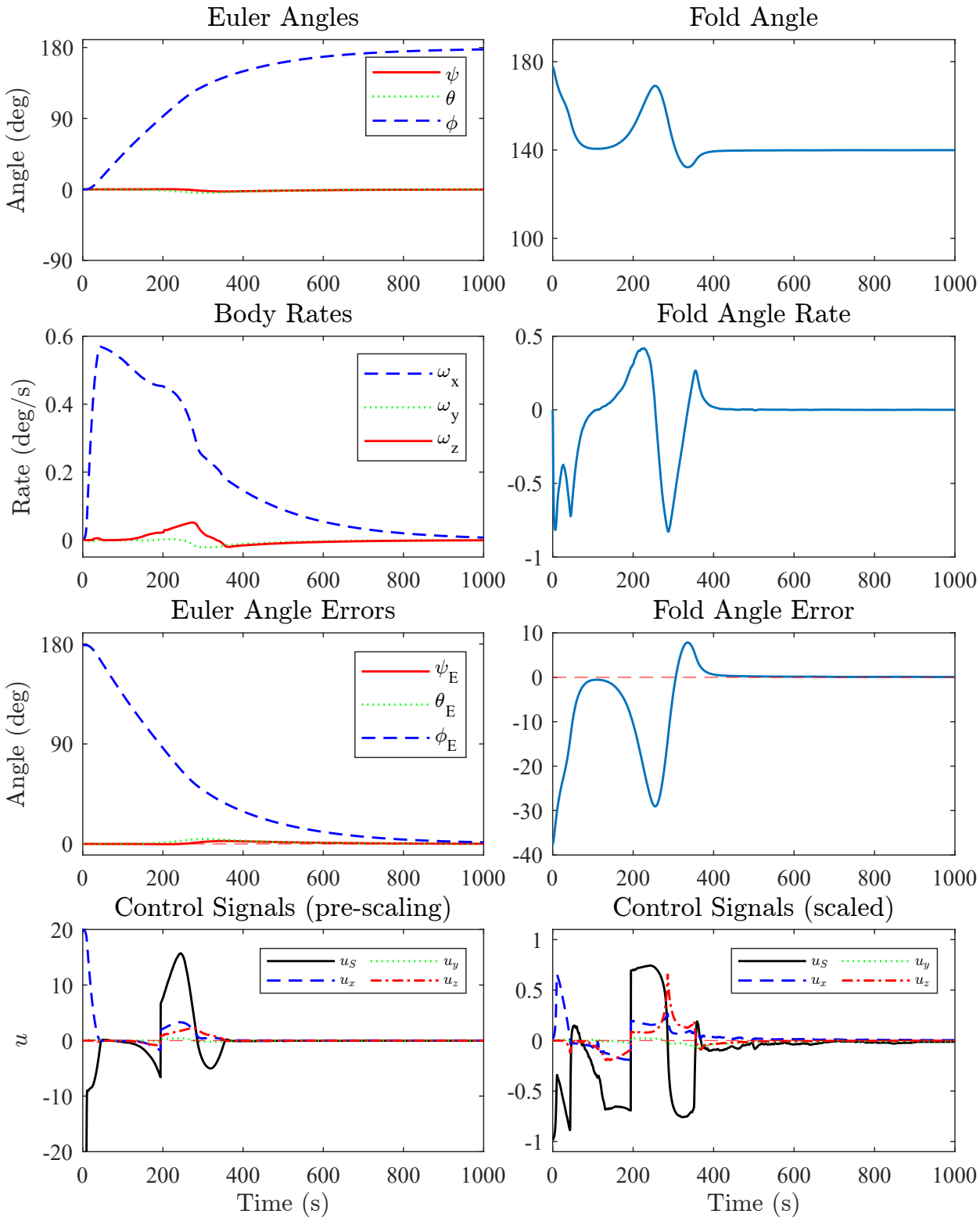

Figure 8: Results of simulation for a 180° manoeuvre around the body x-axis and simultaneous shape reconfiguration

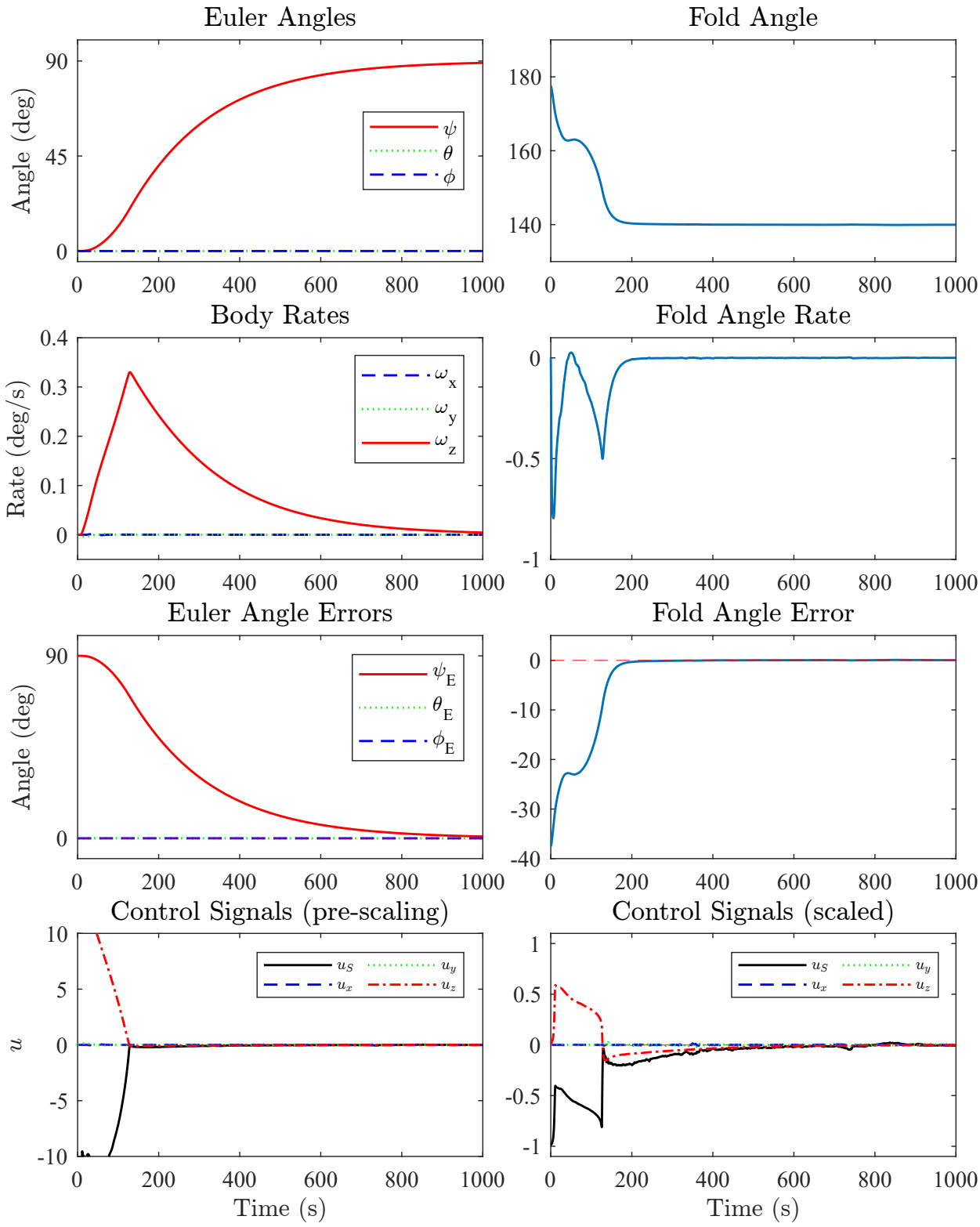

Figure 9: Results of simulation for a 90° manoeuvre around the z-axis and simultaneous shape reconfiguration

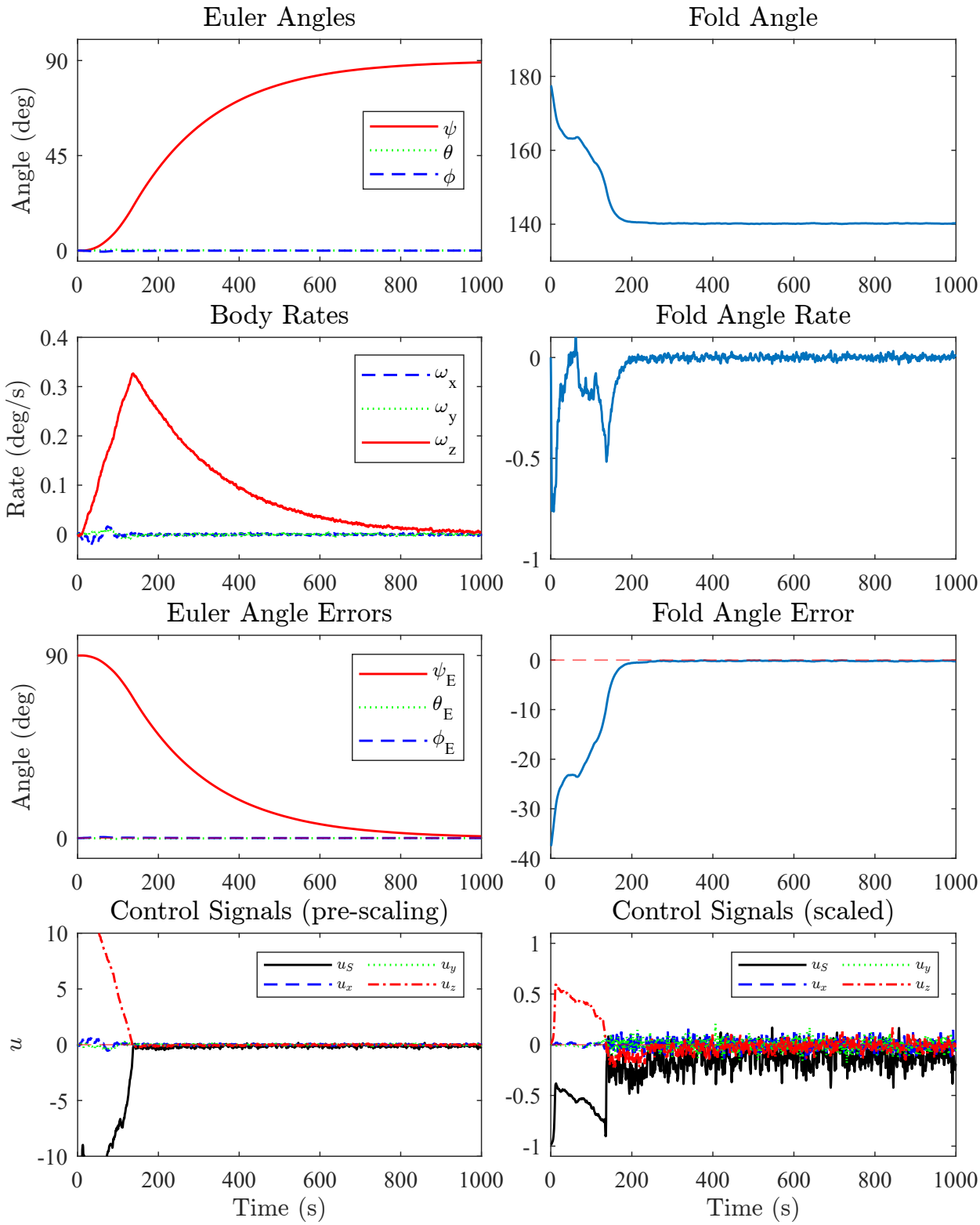

Figure 10: Results of simulation for a 90° manoeuvre around the z-axis and simultaneous shape reconfiguration, with random perturbations added to panel forces.

direction by around 5-10°. Thus the panel forces now have a significant perturbation from the calculated ideal forces of Eq. 2 which is updated on each timestep of the simulation.

Results of this simulation are shown in Fig. 10. Despite the panel force perturbations, the results overall conform with the previous simulation. The change in the panel forces causes some noise to be seen in the body rates and fold angle rate, though it can clearly be seen that the controller is compensating for these effects, as confirmed by the significant variation in the control signals observed beyond around 180s in Fig. 10. The final error in folding angle for the previous simulation (Fig. 9) was approximately 0.03 degrees, while now the error is found be approximately 0.2 degrees, so there has been some loss in accuracy of the shape control and panel orientation due to the included perturbations.

5. Conclusion

An integrated shape attitude closed feedback control law has been presented and demonstrated for a Miura-fold pattern OrigamiSat. The proposed control law is seen to perform well, with 3-axis attitude control achievable, and shape reconfiguration possible between $\Phi_M = 180°$ and 114° when folding towards the incident sunlight, and in the full range when folding away from the Sun. While an ideal model has been assumed, in which panel reflectivities are controllable between 0 and 1, the principle of variable reflectivity as a form of attitude and shape control has been demonstrated. In particular, the proposed strategy of combining the shape and attitude control patterns from the separate closed loop controllers has proven to be a simple and effective method, where judicious selection of the control gains is found to lead to the controller performing a natural trade-off between these competing objectives.

In practice the controller will need to overcome a number of disturbances and effects which are not considered in the model used here, such as membrane curvature, wrinkling or vibration, and furthermore sensor performance and noise will need to be taken into account in future demonstrations. A first step was taken to demonstrate the performance of the controller in the presence of these effects by repeating a simulation with the addition of unknown, random perturbations to the panel forces at each simulation timestep. The controller was found to easily overcome these perturbations, though the robustness of the system will require further study.

The feasibility of the OrigamiSat concept is mostly demonstrated by previous solar sailing missions, e.g IKAROS [2], Nanosail-D[19], and Lightsail [20]. RCD devices and attitude control similarly were demonstrated by the IKAROS mission and have been well studied. The main difference and new technology to be tested for OrigamiSats is the hinges and potential torque required to overcome the bending resistance of the hinge material. Previous research (Ref. [1]) has demonstrated that for a given hinge material and thickness, a minimum panel size would be required to successfully perform shape reconfiguration, though beyond this size there is favourable length-scaling and the hinge resistance becomes negligible. A further practical consideration is the packaging and deploying of the spacecraft, though membrane packaging and deployment has been successfully demonstrated by the previously mentioned missions and extensive ground testing. For the OrigamiSat concept, it could be feasible to launch a folded origami sat and then deploy in space, for a design capable of being folded to fit within a launch vehicle fairing. Another potential strategy could be to assemble a larger OrigamiSat from separately deployed sails, or 3D-print a rigidising frame directly onto membrane in-orbit.

The proposed strategy could likely be applied to other OrigamiSat designs, though the predefined reflectivity patterns would need to be known in advance for each degree of freedom of the origami pattern. Indeed, for many origami patterns it is likely that the patterns required to enact a fold around a certain edge will change depending on the sail attitude, and thus could not be predefined in the same way as was possible here for the Miura sail. In this case it may be possible to employ some form of model predictive control, whereby at each timestep the set or a subset of the possible reflectivity patterns are tested through simulation to determine which degrees of freedom are acted upon by different combinations. The reflectivity pattern best matching an optimal trajectory to the desired configuration could then be selected. While such a strategy could be promising, the computational power required to test every possible combination of panel reflectivities would be large and would not scale well for an increased number of panels.

Acknowledgements

CM was supported by the Royal Academy of Engineering under the Chair in Emerging Technologies scheme. SS and PP were funded by the Connected Everything II feasibility study Grant Ref: EP/S036113/1 in partnership with the Japan Aerospace Exploration Agency and Oxford Space Systems, in collaboration with the University of Glasgow.

References

[1] A. Russo, B. Robb, S. Soldini, P. Paoletti, C. R. McInnes, J. Reveles, A. K. Sugihara, S. Bonardi, O. Mori, Mechanical Design of Self-reconfiguring 4D-printed OrigamiSat: a New Concept for Solar Sailing, Frontiers in Space Technologies 3 (2022).

[2] Y. Tsuda, O. Mori, R. Funase, H. Sawada, T. Yamamoto, T. Saiki, T. Endo, J. Kawaguchi, Flight status of IKAROS deep space solar sail demonstrator, Acta Astronautica 69 (9-10) (2011) 833–840. doi:10.1016/j.actaastro.2011.06.005.

[3] D. Ma, J. Murray, J. N. Munday, Controllable Propulsion by Light: Steering a Solar Sail via Tunable Radiation Pressure, Advanced Optical Materials 5 (4) (2017). doi:10.1002/adom.201600668.

[4] M. Bassetto, L. Niccolai, L. Boni, G. Mengali, A. A. Quarta, C. Circi, S. Pizzurro, M. Pizzarelli, R. C. Pellegrini, E. Cavallini, Sliding mode control for attitude maneuvers of Helianthus solar sail, Acta Astronautica 198 (May) (2022) 100–110. doi:10.1016/j.actaastro.2022.05.043.
URL `https://doi.org/10.1016/j.actaastro.2022.05.043`

[5] L. Boni, M. Bassetto, L. Niccolai, G. Mengali, A. A. Quarta, C. Circi, R. C. Pellegrini, E. Cavallini, Structural response of Helianthus solar sail during attitude maneuvers, Aerospace Science and Technology 133 (2023) 108152. doi:10.1016/j.ast.2023.108152.
URL `https://doi.org/10.1016/j.ast.2023.108152`

[6] K. Xie, C. Li, S. Sun, C.-y. Nam, Y. Shi, H. Wang, W. Duan, Z. Ren, P. Yan, Electrothermally Driven Reconfiguration of Microrobotic Beam Structures for the ChipSail System (2023).

[7] Z. Ren, J. Yuan, X. Su, H. Sun, R. Galos, Y. Shi, S. Mangla, M. Lu, F. Camino, Vertical deployment of multilayered metallic microstructures with high area-to-mass ratios by thermal actuation, Journal of Micro and Nano-Manufacturing 7 (3) (2019). doi:10.1115/1.4043987.

[8] F. Trovarelli, M. McRobb, Z. Hu, C. R. McInnes, Attitude control of an underactuated planar multibody system using momentum preserving internal torques, in: AIAA Scitech 2020 Forum, Orlando, FL, 2020. doi:10.2514/6.2020-1686.

[9] F. Trovarelli, Strategies for Attitude Control of Reconfigurable Modular Spacecraft, Msc(res) thesis, The University of Glasgow (2022).

[10] S. Gong, H. Gong, P. Shi, Shape-based approach to attitude motion planning of reconfigurable spacecraft, Advances in Space Research 70 (5) (2022) 1285–1296. doi:10.1016/j.asr.2022.06.004.

[11] H. Gong, S. Gong, Design of foldable PCBSat enabling three-axis attitude control, Acta Astronautica 192 (September 2021) (2022) 291–300. doi:10.1016/j.actaastro.2021.12.004.

[12] H. Ashrafiuon, R. S. Erwin, Sliding mode control of underactuated multibody systems and its application to shape change control, International Journal of Control 81 (12) (2008) 1849–1858. doi:10.1080/00207170801910409.

[13] H. Gong, S. Gong, D. Liu, Attitude dynamics and control of solar sail with multibody structure, Advances in Space Research 69 (1) (2022) 609–619. doi:10.1016/j.asr.2021.10.012.

[14] T. Sinn, M. Vasile, Multibody dynamics for biologically inspired smart space structure, in: AIAA Spacecraft Structures Conference, National Harbor, Maryland, 2014. doi:10.2514/6.2014-1364.

[15] A. A. Shabana, Computational Dynamics, 3rd Edition, Wiley, 2010.

[16] A. Borggräfe, J. Heiligers, M. Ceriotti, C. R. McInnes, Attitude control of large gossamer spacecraft using surface reflectivity modulation, in: International Astronautical Congress, 2014, pp. 1753–1759. arXiv:0812.0143v2, doi:10.1016/j.buildenv.2006.10.027.

[17] B. Robb, M. McRobb, G. Bailet, J. Beeley, C. R. McInnes, Distributed Magnetic Attitude Control for Large Space Structures, Acta Astronautica 198 (September) (2022) 587–605.

[18] G. Ellis, Control System Design Guide, 1st Edition, Elsevier Inc., 2012. doi:10.1016/C2010-0-65994-3.

[19] D. C. Alhorn, J. P. Casas, E. F. Agasid, C. L. Adams, G. Laue, C. Kitts, S. O'Brien, NanoSail-D: The Small Satellite That Could!, 25th Annual AIAA/USU Conference on Small Satellites (2011) 1–15.

[20] R. Ridenoure, R. Munakata, A. Diaz, LightSail Program Status: One Down, One to Go, 29th AIAA/USU Conference on Small Satellites (626) (2015) 1–50.